Published by
NIGERIAN SOCIETY OF PHYSICAL SCIENCES
Available online @ https://journal.nsps.org.ng/index.php/jnsps

J. Nig. Soc. Phys. Sci. 8 (2026) 3078

Journal of the Nigerian Society of Physical Sciences

Sustainable photocatalytic degradation of methylene blue dye induced through biogenic synthesis of metal oxide nanoparticles mediated orange peel extract

Oyesolape Basirat Akinsipo (Oyelaja)*, Abosede Adejoke Badeji, Victor Olamilekan Folorunsho, Abiola Kareem Asunmo, Olamilekan Emmanuel Agboola

Department of Chemical Sciences, College of Science and Information Technology, Ijagun, PMB 2118, Tai Solarin University of Education, Ijebu-Ode, Ogun State, Nigeria.

Abstract

Synthetic azo dyes, widely used in various industries, pose serious environmental and health risks due to their toxic, non-biodegradable, and carcinogenic nature when released into aquatic ecosystems. This research focuses on synthesizing and evaluating orange peel-green synthesized zinc oxide nanoparticles (OZONp) as an efficient photocatalytic nanomaterial for the degradation of methylene blue (MB) dye. OZONp were prepared at different concentrations (0.01-0.1 M) of zinc acetate dihydrate and characterised through UV-VIS spectrophotometer, Fourier Transform Infrared (FT-IR) and Scanning Electron Microscope (SEM). The molecular insight into the geometry of phytochemicals of orange peel extract in the activity of OZONp was studied using density functional theory computations. The morphology variations driven by the precursor concentration using SEM analysis were not regular as it changed to irregular spheres and nanoflowers. UV-Vis spectra proved the formation of OZONp with an absorption band within 250-320 nm. FTIR spectra signals the presence of phytochemicals that mediate reduction and stabilization. Photocatalytic degradation experiments of various MB concentrations (5-50 mgL^{-1}), revealed that the higher the Zinc salt concentration, the higher the MB degraded, especially under 0.1 M and 5 mgL^{-1} of the dye MB. Pseudo- first-order reaction behavior was followed by kinetic modelling with R^2 values greater than or equal to 0.99. Computational studies revealed that orange peel extract has ferulic acid, hesperidin and narirutin which have desirable electronic properties, which makes them good candidates in the formation of OZONp. The properties are probably beneficial to the process of photocatalytic degradation of methylene blue dye, especially when light is present.

DOI:10.46481/jnsps.2026.3078

Keywords: Green synthesis, Zinc oxide nanoparticles, Photocatalytic degradation, Orange peel, Methylene blue dye

Article History :
Received: 11 August 2025
Received in revised form: 03 February 2026
Accepted for publication: 08 February 2026
Available online: 11 April 2026

Communicated by: E. Etim

1. Introduction

Synthetic dyes (azo dyes primarily) are used in large scale in textile, cosmetic, pharmaceutical and food manufacturing industries. Nevertheless, when they are released into aquatic ecosystems, they carry lots of environmental and health threats [1]. These dyes tend to be non-biodegradable, toxic, and carcinogenic, causing depletion of oxygen, eutrophication, and altering the aquatic life. Even low levels of them can give water strong coloring, which influences photosynthesis and the quality of water [2, 3]. Conventional methods of wastewater treatment like coagulation, flocculation, filtration, and biologi-

*Corresponding author: Tel.: +234-816-661-7462
Email address: solape2010@gmail.com; akinsipoob@tasued.edu.ng (Oyesolape Basirat Akinsipo (Oyelaja))

cal degradation fail to perform well in the degradation of complex molecules like dyes [4]. A good number of dyes survive microbial degradation, and they are persistent in the treated effluents. Besides, such techniques tend to produce secondary pollutants, use a lot of energy, and utilize infrastructure that is expensive to use at between scales, which renders the technique not sustainable at those scales [5].

The future of nanotechnology is bright in the field of dye remediation. Probably the best-known photocatalytic material with metal oxide nanoparticles is zinc oxide (ZnO), which shows good photocatalytic behavior because of the large surface area, stability, and possibility of transforming into active oxygen species in the presence of light. These nanoparticles have the potential to degrade the molecules of dye to non-toxic sub-products, which is more efficient and planet-friendly [6].

The concept of green synthesis of nanoparticles exploits natural agents like plant extracts, microbes, and biowastes in the reduction of metal salts into nanoparticle form. Green synthesis is cheap, non-hazardous, energy-efficient, and eco-friendly as compared to the use of chemical reactions [7]. It does not require any unsafe reagents and does not hinder large-scale production with low waste [8]. The orange peel extract contains flavonoids, phenolics, terpenoids, and ascorbic acid as natural reducing and stabilizing agents in the preparation of nanoparticles. Not only does the use of orange peel valorize agricultural waste, but it also increases the biocompatibility and stability of the resultant nanoparticles [9]. The example of its antioxidant and antimicrobial activities also works on the functional performance of OZONp nanoparticles in dye degradation.

The purpose of this study is to synthesize OZONp using orange peel extract through a green route and also test their effectiveness in removing synthetic dyes in wastewater. The implications are that it can encourage eco-friendly nanotechnology via biowaste use, resolve the drawbacks of traditional treatment procedures, give a boost to environmental remediation with the help of biogenic Zinc oxide nanoparticles, and support a circular economy via upcycling of waste into usable materials.

2. Materials and methods

2.1. Purchase, cleaning and preparation of orange peel extract

Citrus sinensis (orange) fruit peels were obtained as fresh materials supplied by juice traders in Lagos, Nigeria. The peels were first washed using distilled water in order to get rid of dust and contaminant substances on the surface before air-drying in ambient temperature (25-30 °C) over a period of 48 hours. A mechanical blender was employed to convert the dry peels into powder.

The extract was prepared by adding 100 mL of deionized water to 10 g of powdered peel and boiling at 60 °C under constant stirring with a magnetic stirrer for 1 hour. The mixture was filtered after cooling to room temperature with Whatman No. 1 filter paper. The filtrate was obtained and kept at 4 °C to be employed as the precipitating and stabilising agent in the preparation of the nanoparticle.

2.2. Phytofabrication of OZONp

The green synthesis of OZONp, as shown in Figure 1, was carried out using $Zn(C_2H_3O_2)_2 2H_2O$ as the source of zinc oxide. The mixture was vigorously stirred by adding 50 mL of orange peel extract to the 100 mL solution of zinc acetate dihydrate drop by drop. The mixture was adjusted to near pH 10 with 1M NaOH to support the formation of nanoparticles. The mixture was kept at 60 °C for 1 hr with constant stirring, and the formation of white precipitate occurred. This precipitate was centrifuged at 3000 rpm/15 min and washed three times with water and distilled water to remove any unbound impurities. The obtained nanoparticles were dried overnight in an oven at 60 °C. To enhance its crystallinity and give a Zinc oxide nanopowder, the dried product was calcined at 350 °C in muffle furnace after 2 hours.

2.3. Characterization of zinc oxide nanoparticles

The characterization of OZONp was done to prove the success of the synthesis, as well as determine physicochemical parameters of the nanoparticles. Instrumental analysis of the nanoparticles in the spectral region 200-800 nm was done on a UV-Vis spectrophotometer (Shimadzu UV-2600). The band gap was estimated by Tauc plot extrapolation at the absorption peak. Fourier Transform Infrared spectroscopy (FTIR) analysis was carried out on an FTIR spectrometer (PerkinElmer Spectrum Two) to determine the functional groups that participate in the formation of nanoparticles. The spectra were scanned between 4000 cm^{-1} and 400 cm^{-1}. The presence of bioactive compounds in the peel extract was observed on OZONp surfaces with peaks that meet hydroxyl, carboxyl and flavonoid. Surface morphology and particle size analysis was done under Scanning Electron Microscopy (SEM) (SEM Model Phenom ProX by phenom World Einhoven, The Netherlands).

2.4. Photocatalytic degradation of methylene blue dye

In order to probe the photocatalytic activity of the green synthesized OZONp, a degradation experiment was carried out using methylene blue (MB) dye solutions. 100 mg of MB dye was dissolved in 1 L of distilled water to prepare a stock solution. 100 mg of MB dye was dissolved in 1 L of distilled water to prepare a stock solution. The stock solution was used to prepare various lower concentrations of 5 mgL^{-1} , 10 mgL^{-1} , 20 mgL^{-1} and 50 mgL^{-1} using serial dilution. To monitor the photocatalytic activity of OZONp, 100 ml of each dye solution was taken in a beaker along with 2.24 g of nanoparticles and kept under sunlight along with continuous stirring. The absorbance was then taken at definite time intervals, and the degradation efficiency was calculated as:

$$\text{Degradation efficiency } (\%) = \frac{(C_0 - C_t)}{C_0 \times 100},$$

where, C_0 is the initial concentration, and C_t is the concentration of methylene blue dye at time (t).

Aliquots of each reaction mixture were collected at regular time intervals (15, 30, 45 minutes, and 1 hour). The samples were allowed to settle, which helped the nanoparticles separate.

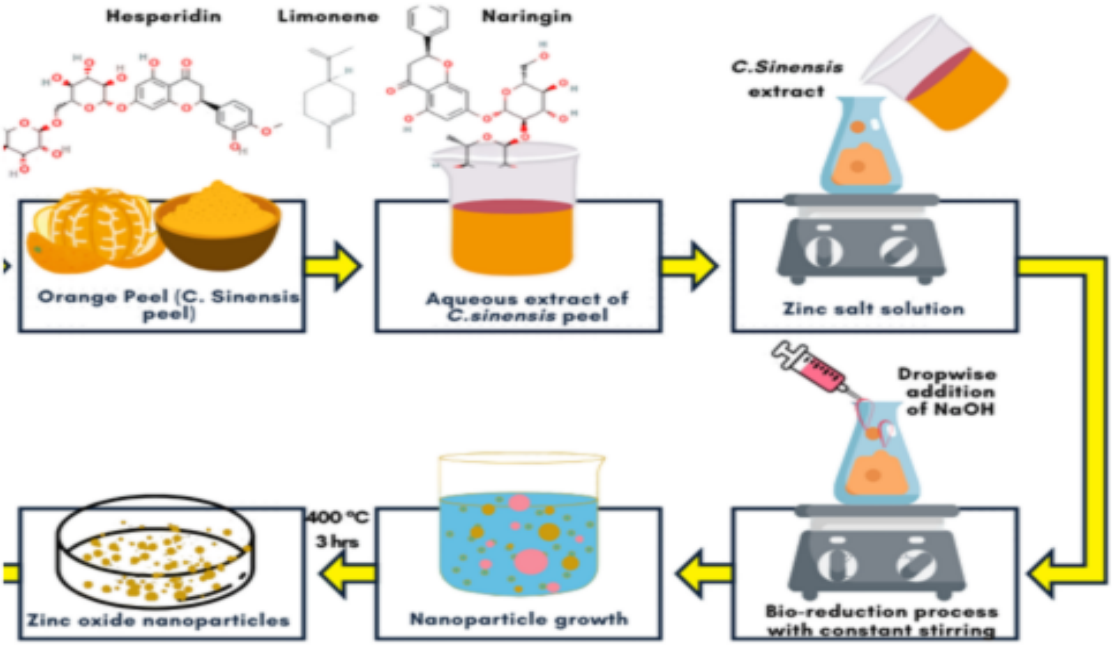

Figure 1: Schematic illustration of the phytofabrication of OZONp.

Then, the UV-visible absorption spectra were recorded for each sample at the appropriate times. Particularly, the absorbance measures at a wavelength of 665 nm were recorded and observed over time to observe any alterations in the course of this reaction mixture. MB dye percentage degradation was also calculated.

2.5. Computational method

Geometric optimization of the major phytochemicals that occur in orange peel (limonene, ferulic acid, hesperidin, and narirutin) was conducted using density functional theory (DFT) calculations. The M06-2x hybrid functional [10] in combination with the def2-TZVP basis set [11] was employed for all atoms (carbon, hydrogen, and oxygen). Calculations were performed and collected with the Gaussian 16 software package accessed on the Lengau cluster in the Centre for High Performance Computing (CHPC) in Cape Town, South Africa. Molecular structures and input files were generated using GaussView 6.0.16 [12], where visualization of pre-optimization and post-optimization geometries was also carried out. The developed 3D simulations of the optimised phytochemicals were also well represented using ChemCraft [13] to improve readability. The preferential choice of the M06-2x hybrid functional as the best performer in the description of both non-covalent interactions, dispersion forces, and medium-range correlation effects was due to their importance in the accurate determination of the electronic properties of phytochemicals and their possible interactions with metal ions. The def2-TZVP basis set was selected in order to offer a balanced trade-off between computational efficiency and chemical accuracy to systems comprising carbon, hydrogen, and oxygen atoms. This degree of theory is widely applicable in the study of organic molecules that are under a high degree of 8 concurrence along with multi-functional groups, and thus is specifically applicable to the flavonoids and phenolic acids that are found in orange peel extract.

2.5.1. Frontier molecular orbital (FMO) analysis and quantum chemical descriptors

Frontier Molecular Orbital (FMO) is essential in understanding the electronic, optical and reactivity property of organic molecules [14–18]. The highest occupied molecular orbital (HOMO) energy, lowest unoccupied molecular orbital (LUMO) energy, and the HOMO-LUMO energy gap (Delta Eg) are especially useful as parameters in the identification of reactive sites in systems of π electrons [15]. The HOMO energy is a measure of the molecule selling of electron density, and is analogous to the ionization potential (IP), with high HOMO energies signifying increased receptivities to donation by electrophiles. On the other hand, the LUMO energy is a measure of the degree of acceptance of electrons by a molecule and the lower the LUMO energy, the further susceptible the molecule will be to nucleophilic attacks [17]. The energy difference of the HOMO-LUMO determines the energy of electronic transition, and smaller energy gaps denote higher molecular reactivity and lower kinetic stability [18]. In this work, FMO analysis was done to analyse the optimized molecular geometries of the phytochemicals examined, and their HOMO, LUMO and Eg values were used to evaluate the reactivity of some of the investigated phytochemicals and give an indication of the possible interaction locations and reactivity patterns.

Moreover, an assessment of a molecule has been done with several quantum chemical descriptors as well as chemical activity and stability structure [19–23]. These are the global hardness (η), global softness (σ), electronegativity (χ) and the electrophilicity index (ω). Hardness and softness are able to reveal how far off the molecule is to changes within the context of an electron density [24], whereas electronegativity expresses how the same is able to draw in the electrons [25]. The index of electrophilicity is the measure of the reactivity of the molecule with nucleophiles or species rich in electrons [9]. These descriptors were calculated using the formulas described in the literature [17–20, 22].

2.5.2. *Molecular electrostatic potential (MESP) map*

Molecular Electrostatic Potential (MESP) map is a significant tool to visualize the chemical reactivity of molecules, especially in the context of electrophilic and nucleophilic reactions [23–25]. In this research, the MESP diagrams of the phytochemicals were calculated and displayed through the GaussView program interface [12]. This color gradient map relates to the different degrees of an electrostatic potential. Blue color codes are with maximum positive potential likely to react with nucleophilic centers, whereas red color codes are of maximum negative charge, mostly prone to electrophilic attack. Green indicates neutral areas of electrostatic potential. The MESP map assists in identifying possible reactive sites of the molecule.

3. Results and discussion

3.1. *Production and visual inspection of ZnO nanoparticles*

Green synthesis of OZONp through the use of *Citrus sinensis* peel extract produced a pale white precipitate (Figure 2), affirming the success of ZnO production. Zn^{2+} ions became precipitated and stabilized in the presence of the phytochemicals (flavonoids, terpenoids, and phenolic acids) in the extract, causing the solution to turn milky white during the synthesis.

Figure 2: Zinc oxide nanoparticles.

3.2. *UV-visible spectrophotometric analysis*

The UV-visible spectrum of the different OZONp prepared with sweet orange peel extract and four different concentrations of zinc salt (Figure 3b-3e) showed sharp band absorption occurring in the 250-280 nm range, indicating a blue-shift as compared to the normal ZnO band-edge absorption (350-380 nm). With a nanoparticle concentration of 0.01 M (Figure 3a), only a shallow peak and a poorly defined absorption were recorded near 320 nm, showing low nanoparticle yield or non-constructions of crystallization, potentially caused by an inadequate number of Zn^{2+} ions to initiate effective nucleation [26]. Remarkably, the samples made at higher concentrations of zinc salts (0.05 M and 0.1 M; Figure 3c and 3e) had an extra weak absorption band at a wavelength close to 400 nm. This secondary absorption characteristic may be explained by: (i) surface defect states due to oxygen vacancies and zinc interstitials, which are more numerous in highly crystalline nanoparticles; (ii) residual organic compounds of the orange peel extract which are not desorbed and which thus remain on the surface of the nanoparticle, especially at high concentrations of the precursor when more phytochemical-metal complexation is observed; and (iii) potential light scattering effects of higher particle aggregates or nanoflower morphologies that are seen at these concentrations during SEM The rise of the intensity of this band is associated with the rising concentration of the precursors indicating the increase of the level of surface modification and/or the creation of structural defects during synthesis. In the past four years, most green-synthesized ZnO NPs have reported a peak-absorption of between 353 and 364 nm; e.g., ZnO prepared using Justicia adhatoda extract reached a peak of 353 nm (bandgap 3.09 eV), and ZnO prepared using fruit peel extracts such as Wodyetia bifurcata generated peaks between 354 and 364 nm [27]. The blue shift of absorption edge (250-280 nm) over bulk ZnO (350-380 nm) may be due to the comparatively small size of crystallites in SEM analysis (20-65 nm), which is close to the ZnO Bohr exciton radius (around 2.34 nm of the smallest subunits). Furthermore, the powerful effects of surface-bound phytochemicals as capping agents are also a possible cause of the modified optical properties that form surface states that modify the effective band gap [28]. Besides, the flavonoids and polyphenols found in orange peel extract are phytochemicals that act as natural capping agents, which mitigate the surface defect states and help increase the higher-energy absorption edge [29]. Therefore, the UV-Vis absorption spectra indicate that ultra-small and well-stabilized ZnO nanoparticles were produced with high optical activity and therefore can be employed to serve UV-screening and antimicrobial purposes considering the robust UV absorption and the likely large surface area. These results also confirm that green routes to prepare OZONp with orange peel are not only a clean way to make nanoparticles and result in dramatic tuning of optical properties by reducing size and stabilizing with phytochemicals.

3.3. *FT-IR analysis*

FTIR analysis of the OZONp obtained from different concentrations of zinc acetate dihydrate produced through the use of orange peel extract indicates the presence of observable functional group vibrations of both lattice objects (OZONp) and the phytochemical components of the plant extract used (Figure 4a-4e). FTIR spectra showed sharp signals at 3400 cm^{-1}, O-H stretching vibration of alcohols, phenols; 1630 cm^{-1}, C

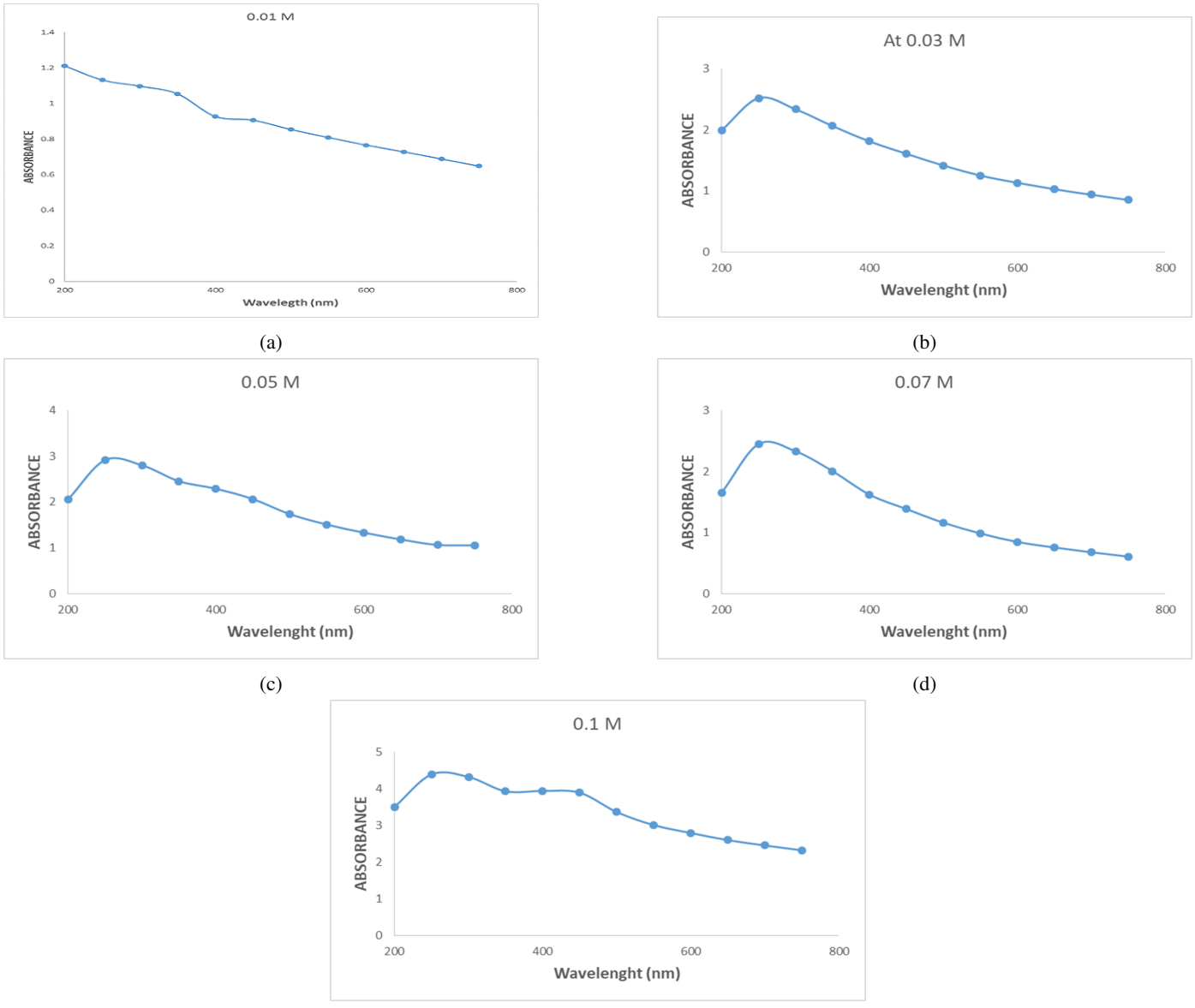

Figure 3: (a-e) shows the UV-visible spectrum of OZONp at 0.01 M, 0.03 M, 0.05 M, 0.07 M, and 0.1 M zinc salt concentrations, respectively. The UV absorption band of the obtained OZONp are found within the ultraviolet spectrum (280 to 380 nm), which is largely related to its wide band gap.

= O stretching vibration of carboxyl acids; 1380 cm^{-1}, C-N stretching vibration of amines; 500-600 cm^{-1}, Zn-O stretching vibration. These functional groups confirm the presence of bioactive compounds from orange peel extract acting as reducing and stabilizing agents. Other peaks at 618.73808 cm^{-1} and 1375.38766 cm^{-1} are associated with Zn-O-H bending vibration and C-N stretching vibrations, respectively. Fine structure gives extrema at 1625 cm^{-1} and 2852 cm^{-1}, which are attributed to C=C stretching and C 13 C stretching vibrations, respectively. These suggest the presence of aromatic and alkyne organic species on the NP surface. In general, FT-IR spectrum shows that the synthesized nanoparticles have a complicated surface chemistry; Zn-O, O-H, Zn-O-H, C-O, C-N, C=C, and $C \equiv C$ functional groups. The results give significant feedback on the composition and properties of the nanoparticles as well as their applicability. The FT-IR pattern of 0.01 M zinc oxide nanoparticles (Figure 4a) exhibits characteristic peaks due to a unique composition and surface features of the studied material. Zn-O lattice vibrations also corresponds to a peak of 454.73 cm^{-1} indicating that the production of OZONp has been successful. Besides that, an intermediate-strong peak at 1364.20 cm^{-1} refers to C-N stretching vibrations, so it is possible to assume that there is nitrogen-containing groups on the surface that might be an indication of potential surface modification or surface functionalization. Additionally, there is a small peak at 1621.39 cm^{-1} which is associated with aromatic C=C stretch-

ing indicating that there is adsorption of organic species onto the surface. This would possibly impact optical and electrical characteristics of the nanoparticles. A wide peak at 3276.32 cm^{-1} is attributed to hydroxyl (O-H) stretching, which demonstrates the presence of the hydroxyl groups on the surface. Comprehensively, the FT-IR data provide interesting information on the surface chemistry with a complicated dynamic between Zn-O, C-N, C=C, and O-H characteristic groups [30]. Figure 4b illustrates the FT-IR of 0.03 M OZONp portraying distinctive functional visions at 417.46 - 1237.48 cm^{-1} that exemplifies a multifaceted nano material chemistry. The highest value of 417.46 cm^{-1} can be attributed to the Zn-O stretching mode and as such confirms that the OZONp has been successfully synthesized. Moreover, a maximum at 514.37 cm^{-1} has been attributed to the Zn-O-H bending vibration, which identifies the fact that the nanoparticle has hydroxyl groups on its surface. Further assessment gives the peaks at 626.19 cm^{-1} and 1144.29 cm^{-1} respectively corresponding to the C-O and C-N stretch vibrations. These findings imply the existence of surface-adsorbed organic species and nitrogen-containing groups bound to the surface [31]. Finally, 1237.48 cm^{-1} peak is assigned to the C=C stretching vibrations (presence of aromatic organic compounds). The FT-IR spectrum of Zinc oxide nanoparticles indicated complex surface chemistry behaviors at 0.05 M (Figure 4c), as evident by distinct absorption bands at 410.00 - 3280.05 cm^{-1}. A prominent peak at 410.00 cm^{-1} is associated with the Zn-O stretching vibration, thereby confirming the successful synthesis of ZnO nanoparticles. Besides, another wide peak of 3280.05 cm^{-1} is associated with O-H stretching vibration which implies the availability of hydroxyl groups on the nanoparticle surface. Further study shows maxima at 518.09 cm^{-1} and 622.46 cm^{-1} refer to the stretching and bending of Zn-O-H and C-O, respectively. These observations imply the existence of surface-adsorbed organic species and possible changes of the surface. The C-N stretching vibration peak at 1384.56 cm^{-1} indicates that there were some nitrogen-containing groups on the surface. A wide range of surface chemistry is indicated in the FT-IR spectrum of 0.07 M zinc oxide nanoparticles (Figure 4d) with discreet absorption peaks of between 499.46 - 3272.60 cm^{-1}. The spectrum reveals successful movement towards the synthesis of ZnO nanoparticles based on the peak at 499.46 cm^{-1} which occurs at the Zn-O stretch. A large peak on the surface at 3272.60 cm^{-1} signifies the existence of hydroxyl groups. Further, the intense bands at 544.19 and 1323.20 cm^{-1} indicate the surface-adsorbed organic and the possible surface modificationity through Zn-O-H bending and C-N stretching. Additional study shows lows at 1591.57 and 2113.40 cm^{-1} showing the presence of aromatic and alkyne organic compounds on the surface. The FT-IR spectrum of synthesized 0.1 M zinc oxide nanoparticle (Figure 4e) shows the characteristic absorption at the spectrum region of 480.82 to 3280.05 cm^{-1} indicating diverse surface chemistry. The was a peak at 480.82 cm^{-1}, which is attributed to the Zn-O stretching vibration and it is an indication of the successful production of nanoparticles of ZnO. A general peak located at 3280.05 cm^{-1} due to O-H stretching vibration predicates the existence of hydroxyl groups on the NP surface. Another peak at 618.73 cm^{-1} and 1375.38 cm^{-1} will represent Zn-O-H bending vibration and C-N stretching vibration. Further interpretation shows a peak at 1625.11 cm^{-1} and 2851.41 cm^{-1}, which is associated with C=C stretching vibration and C=C stretching vibration, respectively. These suggest the presence of aromatic and alkyne organic species on the NP surface. Overall, the FT-IR analysis reveals a complex surface chemistry for the synthesized Nanoparticles, with Zn-O, O-H, Zn-O-H, C-O, C-N, $C = C$, and $C \equiv C$ functional groups. These results give important information regarding the properties of the Nanoparticles and their possible utilization.

3.4. SEM Analysis

In this study, the surface morphology of OZONp prepared at various concentrations of Zn precursor (0.01 M - 0.1 M) by using orange peel extraction as a growth medium was also investigated using Scanning Electron Microscopy (SEM). Typical morphologies were observed with different growth conditions of OZONp (Figure 5a-5e). In the minimum precursor concentration, 0.01 M (Figure 5a), the nanoparticle has a blotchy shape and was irregularly shaped. This shape indicates an incomplete or partial nucleation, which could be caused by the lack of Zn^{2+} ions needed to facilitate the formation of a structure. The green synthesis conditions, which were determined by the presence of phenolic compounds in the orange peels extract, probably led to capping at initial stages, leading to uneven-shaped spherical aggregates. These morphologies were obtained in other studies treated with citrus peel and other plant extracts at low precursor concentration [32].

At 0.03 M OZONp (Figure 5b), the nanoparticles were more rod-like in their shape. This allowed elongated structures to be formed due to the increase in precursor concentration enabling an anisotropic growth behavior. It has been suggested that such nanorods are typically due to c-axis growth relative to the wurtzite hexagonal ZnO crystal lattice and that it responds to the specific binding properties of organic moieties to specific crystal planes [33]. The rod-shaped structure increases the charge separation and movement of electrons, which is advantageous in photocatalytic activity.

At 0.05 M, 0.07 M and 0.1 M OZONp concentration (Figures 5c-5e), samples synthesized at these more concentrated precursor solutions regularly carried the form of nanoflowers, with petal-like flakes emerging off of aggregated centers. These morphological attributes are probably an effect of secondary nucleation and self-assembly of nanosheets accompanied by a capping off with flavonoids and carboxylic acids in the extract [34]. Nanoflowers are also associated with a high surface area which facilitates improved dye adsorption and photocatalytic degradation. The transformation between the spherical to rod to nanoflower structures occurs with the increase of Zn^{2+} concentration, and can be attributed to the subtle balance of availability of ions and nucleation rate and the bio-reduction agent. The morphological transformation with precursor concentration is one of the most commonly reported effects of green synthesised ZnO where the phytochemical content and the rate of reaction dictate the shape modification [35].

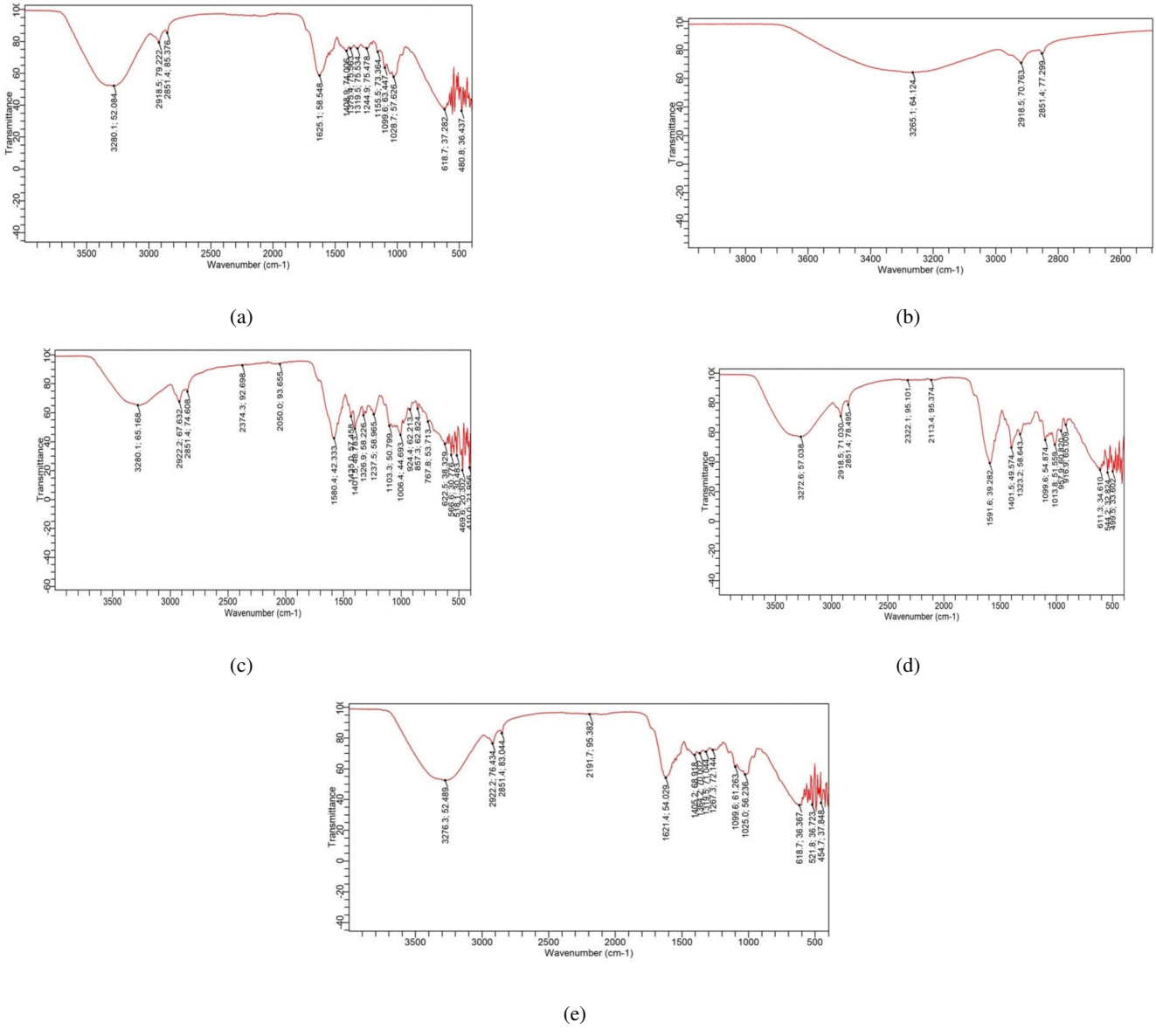

Figure 4: FTIR spectra of OZONp synthesized at different zinc salt concentration, a - e (a) 0.01 M, (b) 0.03 M, (c) 0.05 M, (d) 0.07 M, and (e) 0.1 M respecrively. Key functional groups are labeled, showing Zn-O stretching (400–600 cm^{-1}), C-O stretching (1000–1200 cm^{-1}), C-N stretching (1380 cm^{-1}), C=C stretching (1625 cm^{-1}), and O-H stretching (3200–3400 cm^{-1}).

3.5. Reaction analysis of rate constant and photocatalytic kinetics

The validity of pseudo-first-order kinetic model on the photocatalytic degradation of methylene blue (MB) with ZnO nanoparticles was verified by the goodness of fit (R^2) values. The R^2 values of the ZnO samples were higher than 0.99 at the 5 mgL^{-1} concentration of MB, as it was observed that the reaction kinetics were again very well linear, and highly predictive (Table 1). Nevertheless, at 10 mgL^{-1}, a significant decrease in R^2 values was noticed especially on OZONp synthesized using 0.05 M (0.7564), 0.07 M (0.7354) and 0.1 M (0.6622) precursors. The decreases indicate that ideal pseudo-first-order behavior is not present, perhaps because of active site saturation, aggregation of the particles, or shading of the photons by an excessive number of dye molecules [36]. The intricate trend of R^2 values indicates mechanistic changes in the photocatalytic process that affected its concentration. The pronounced reduction in the value of R^2, especially in cases where higher concentration levels of zinc salt were used to synthesise the samples (0.05-0.1 M) indicates that simple pseudo-first-order kinetics is not obeyed at intermediate dye concentrations (10-20 mgL^{-1}). This is explained by: (i) competitive adsorption between several dye molecules and photogenerated intermediates on active sites which result in mixed-order kinetics; (ii) photon screening effects at intermediate dye concentrations on larger nanoflower structures (generated at higher Zn concentrations) because light is unable to reach the active sites; (iii) accumulation of the degradation intermediates which temporarily occupy

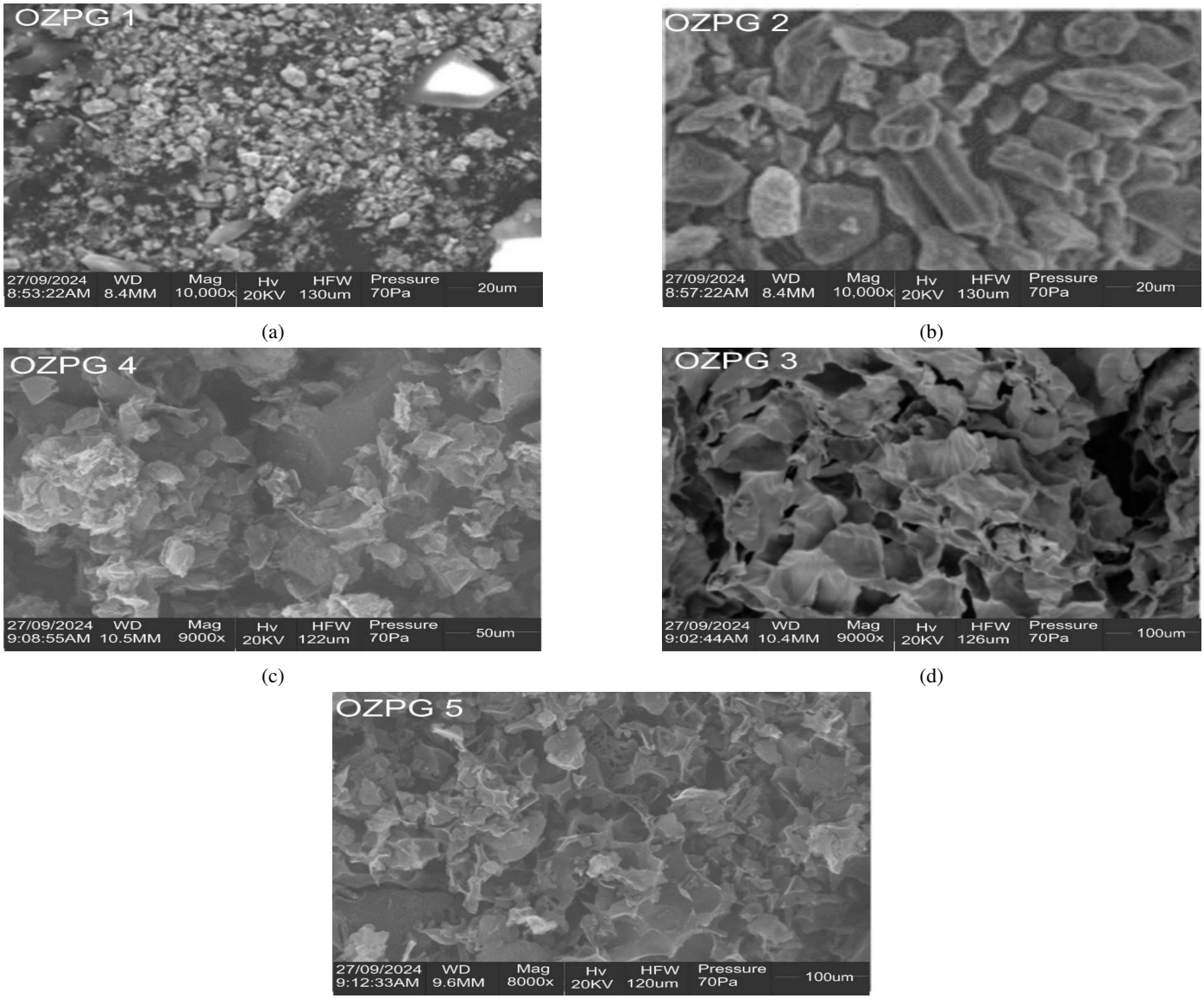

Figure 5: (a-e) SEM Micrographs of Zinc Oxide nanoparticles at different Zn salt concentrations.

catalytic sites. Interestingly, the highest dye concentration (50 mgL^{-1}) give rise to an improvement in the number of R^2 (> 0.94 across all samples), which points to the restoration of pseudo-first-order behavior. Such counterintuitive behavior can be attributed to surface saturation: when the concentration of the dye on the catalyst surface reaches 50 mgL^{-1}, the steady-state has been reached, and the degradation rate can no longer depend on the overall dye concentration, but instead is determined mainly by the absorption of photons and formation of reactive oxygen species. At such saturated conditions, the dynamics reduce to apparent first-order dynamics with respect to surface-bound dye species. This mechanistic complexity defines the necessity to optimize the concentration of catalysts and dyes when applied in practice, and the 0.1 M OZONp concentration exhibits the most consistent results in all the dye concentrations tested.

Whether the photocatalytic degradation of methylene blue (MB) with green-synthesized OZONp follows the pseudo-first-order concept of kinetic degradation was concluded by the experimental fitting to a pseudo-first-order kinetics scheme. The k values as shown in Figure 6a-6e were determined by linear graph of $ln(\frac{C_0}{C_t})$ vs time at the concentration of four MB (5, 10, 20, and 50 mgL^{-1}) in conjunction with OZONp fabricated by various concentrations of zinc salts (0.01- 0.1 M). The findings reveal that concentration of the MB and of Zn precursor exhibited considerable effect on the degradation rate.

Under such condition, the maximum rate constant of degradation was 0.0384 min^{-1} at 10 mgL^{-1} MB using ZnO synthesized using 0.1 M Zn salt, and the lowest value was recorded as 0.0076 min^{-1} at 0.01 M ZnO. The steadily rising k value with increasing ZnO precursor concentration indicates that an increase in precursor concentration induced OZONp with re-

Table 1: Interpretation of R^2 value with kinetic values.

MB Conc. (mgL^{-1})	0.01M Zn	0.03 M Zn	0.05 M Zn	0.07 M Zn	0.1 M Zn
5	0.9942	0.9943	0.9936	0.9943	0.9927
10	0.9502	0.947	0.7564	0.7354	0.6622
20	0.9086	0.8327	0.8392	0.7752	0.9767
50	0.9972	0.9979	0.9416	0.9419	0.9622

spect to quantity and energy of open active sites, crystallinity and improved charge separation phenomena, hence superior photocatalysis ability. These results are consistent with that of Lee *et al.* (2019), who could also notice a maximization of dye degradation when rising ZnO precursor concentrations were used, since particle morphology and photon absorption were bolstered [37]. The dependency of the MB concentration on the rate constants was non-linear. In most OZONp samples, an increase in k values was observed between 5-10 mgL^{-1}, indicating that a moderate concentration of dye favours easy adsorption and reaction of the dye on the catalyst surface. Nevertheless, at increased concentrations (20 and 50 mgL^{-1}), the rate constant decreased or varied, probably because of light screen issues, and saturation in the active sites with excess dye molecules [38]. In one of the examples, the rate constant of 0.03 M OZONp decreased at 20 mgL^{-1} (0.00301 min^{-1}) than at 10 mgL^{-1} (0.0143 min^{-1}), whereas 0.1 M OZONp has a relatively high k (0.0192 min^{-1}) for both concentrations, which demonstrates stronger catalytic activity. The data, in general, show that the concentration of OZONp precursor and dye loading are influential factors in photocatalytic performance. They occurred at OZONp made of 0.1 M Zn salt at 10 mg min^{-1} MB, which proved the need to optimise the parameters of nanoparticle synthesis to suit the intended photocatalytic application.

3.6. Photocatalytic degradation efficiency

Figure 7 and Table 4 present the photocatalytic degradation efficiency of methylene blue with OZONp prepared at various zinc salt concentrations. The efficiency of the degradation rose gradually with the irradiation time across all the metal oxide nanocatalysts, with the highest values achieved after 60 minutes of sun exposure. Table 4 indicates that the degradation efficiency at 60 minutes ranged from 40.5 to 44 %, with slight differences depending on the concentration of the precursor used in OZONp synthesis. The highest degradation efficiency (44 per cent) was displayed by 0.1 M OZONp, then 0.05 M (42.5 per cent), 0.07 M (40 per cent), 0.03 M (40.4 per cent) and 0.01 M (40.5 per cent). These findings suggest that all synthesised OZONp samples are similar in their photocatalytic activity under conditions of the performed experiment, with slightly improved performance at high concentrations of zinc precursors. The almost linear degradation behaviour (Figure 7) in the first 60 minutes indicates that there is no serious deactivation of catalysts or saturation of the active site. The relatively small disparities in performance ($\leq 3.5\%$ variance) across samples can be appropriated to rival elements: whereas bigger precursor concentrations (0.05-0.1 M) generated nanoflower morphologies with conceivably higher surface areas [39, 40], it is also quite possible that larger aggregates can be associated with increased charge carrier recombination and less light penetration into the catalyst suspension [41]. These results in degradation efficiencies of 40-44 % in 60 minutes are comparable to other green-synthesized ZnO photocatalysts found in the literature. An example is that Anik *et al.* (2024) 52% of MB was degraded with Justicia adhatoda-mediated ZnO NPs after 120 minutes under UV irradiation [42] and Rashid *et al.* (2025) 45-60% of degraded ZnO with citrus peel-mediated ZnO under the same conditions [43]. The fact that we used natural sunlight as opposed to controlled UV sources is also significant because a more sustainable and cost-effective approach to real-life applications was employed.

The degradation rate constants and efficiency (Table 2) show some interesting trends. Although the most active time was at 60 minutes in 0.1 M sample, the rate constants were higher in 0.03 M sample at some concentrations of dye as indicated in Table 2, which is why the initial kinetics of degradation might vary with long-term efficiency because the dye adsorption capacity, accumulation of products in the middle of the reaction, and stability of catalysts during the long irradiation might be different at shorter times [44, 45].

On the whole, these results indicate that orange peel-mediated OZONp are good photocatalysts in the degradation of MB using natural sunlight, and their activity is similar or even better than that of other biogenically synthesized metal oxide nanoparticles. This can be attributed to the consistency in the various precursor concentrations implying the strength of the green synthesis process hence can be used in the environment remediation process on a larger scale.

To better understand how the concentration of zinc precursors relates to photocatalytic performance, the rate constants were plotted versus the concentration of zinc salt at each MB concentration used (Figure 8). The graphical analysis shows specific concentration-sensitive behaviors that offer mechanistic information about the photocatalytic process: The rate constant at 5 mgL^{-1} MB (the light blue line) is relatively constant in all concentrations of zinc (0.0085-0.0096 min^{-1}) but slightly higher when zinc concentrations rise between 0.01 M and 0.1 M. Such a low change implies that under a low dye loading, the catalyst quantity or morphology does not restrict the catalyst's photocatalytic performance. In such circumstances, surfactant active sites become surplus as compared to dye molecules, and the rate of degradation is mainly determined by the concentration of dye instead of the characteristics of the catalysts [44]. The rate constant increases dramatically and almost exponentially at 10 mgL^{-1} MB (dark blue line) with a value of 0.0076 min^{-1} at 0.01 M and a value of 0.0384 min^{-1} at 0.1 M, and this

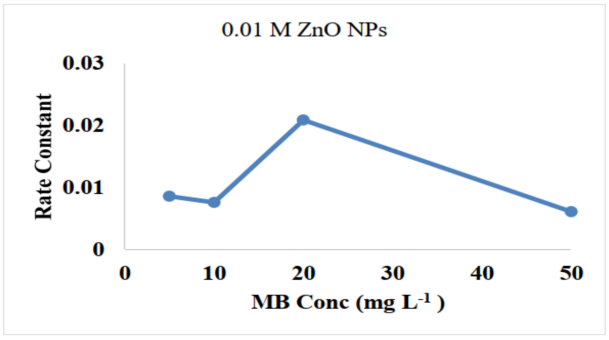

(a)

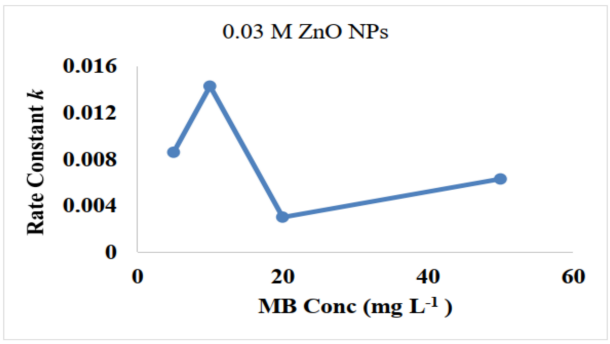

(b)

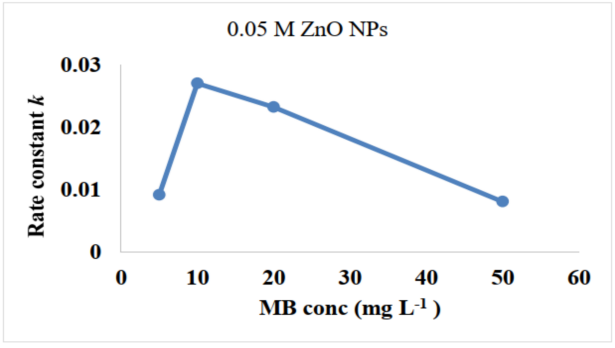

(c)

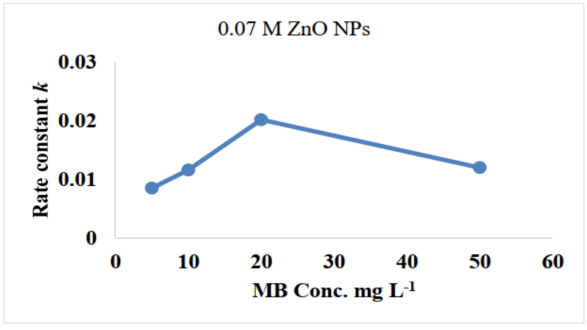

(d)

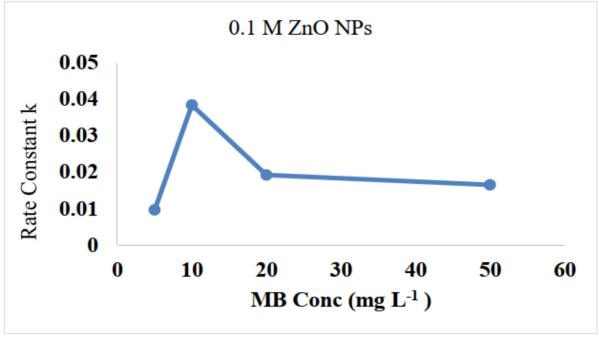

(e)

Figure 6: (a-e) The k values of different MB concentrations at different Zn nanoparticles concentration.

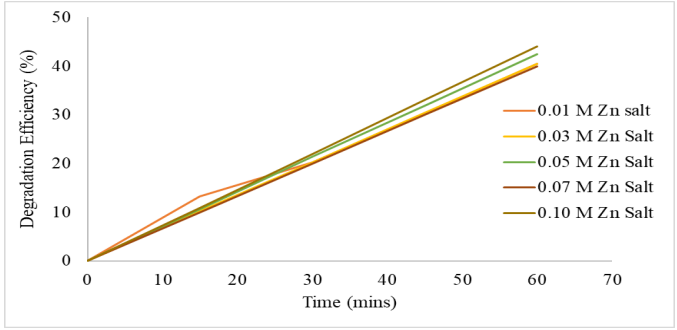

Figure 7: The k values of different MB concentrations at different Zn nanoparticle concentrations.

is a great example of a nearly 5-fold change. This concentration is the optimum trace of dye to catalyst ratio, whereby the higher the concentration of zinc precursor, the higher the level of performance in photocatalysts. This improvement is due to: (i) transformation of disordered aggregates into regular nanoflower structures at higher concentrations of Zn (as found in SEM analysis, subsection 3.4) which offer a larger surface area and a larger number of active sites; (ii) increased crystallinity and minimized defect density; (iii) increased light harvesting capacity of the hierarchical nanoflower structures [39]. At 20 mgL^{-1} MB, a prominent non-monotonic tendency is observed, and the rate constant decreases at the start of the experiment (0.0209 min^{-1}, 0.01 M) to the lowest point of 0.00301 min^{-1} (0.03 M), and then rises rapidly to 0.0232 min^{-1} (0.05 M), and it does not change much further. This deviating trend at a 0.03 M concentration, in which rod-like structures predominate, indicates un-

Table 2: Effect of MB Concentration on Rate constant K (min^{-1}).

MB Conc. (mgL^{-1})	0.01M	0.03 M	0.05 M	0.07 M	0.1 M
5	0.0086	0.0086	0.0092	0.0085	0.0096
10	0.0076	0.0143	0.027	0.0116	0.0384
20	0.0209	0.00301	0.0232	0.0202	0.0192
50	0.0061	0.0063	0.0081	0.012	0.0165

desired interactions at this particular dye-to-catalyst ratio. They could be due to: (i) anisotropic rod morphology can support dye molecule aggregation/stacking on individual crystal faces, blocking active sites; (ii) the one-dimensional geometry can impose diffusion constraints on reactants and products; or (iii) the aspect ratio of nanorods may create diffusion barriers to reactants and products [40]. The transition to nanoflower morphologies at 0.05 M is associated with the recovery and it seems to be offering a superior performance at this dye loading. The maximum dye concentration (50 mgL^{-1} MB) is observed to have a progressive effect on the rate constant at this point (0.0061 to 0.0165 min^{-1}) but not as significant as at 10 mgL^{-1}. The reduced response can be attributed to inherent constraints caused by high dye loading: (i) high dye loading causes strong light screening effects, some of the incident photons are absorbed by excess dye molecules and thus do not reach the catalyst surface; (ii) high dye loading leads to competitive adsorption, resulting in surface saturation; and (iii) high dye loading causes the build-up of degradation intermediates, which occupy active sites [45, 46]. In such circumstances, the best nanoflower morphologies that are obtained in 0.1 M are not able to surmount the mass transfer and light penetration constraints. This is very much justified by the fact that 0.1 M zinc salt converges trends at that point and all the MB concentrations are performing better or best thus making the preferred conditions of synthesis of OZONp. Graphical analysis also reveals that the crucial point is the concentration of the dye matches the loading of the catalyst in the real world situation. The same catalyst that works well at 10 mgL^{-1} (k = 0.0384 min^{-1}) has only moderate activity at 50 mgL^{-1} (k = 0.0165 min^{-1}), thus the need to optimize the process according to the particular characteristics of the actual wastewater.

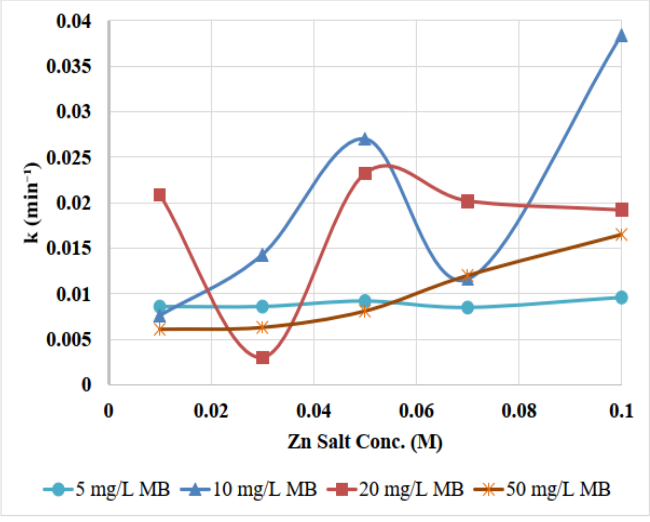

Figure 8: The influence of the concentration of zinc salt on the rate constants of the photocatalytic reaction at varying concentrations of methylene blue. The plot depicts the concentration-dependent behaviors: almost constant performance of 5 mgL^{-1} MB, exponential-like behavior of 10 mgL^{-1} MB, non-monotonic trend with irregular minimum at 0.03 M of 20 mgL^{-1} MB, and linear behavior at 50 mgL^{-1} MB.

3.7. Computational analysis

3.7.1. Frontier molecular orbital analysis and quantum descriptor analysis of the major phytochemicals in orange peel

Although the main photocatalytic agent for MB degradation is the ZnO nanoparticles, the phytochemicals found in the orange peel extract have crucial functions other than the promotion of synthesis. Organic compounds were fixed to the OZONp surface even after calcinations at temperatures up to 350 °C, as was confirmed by the C=C, C-O, and C-N functional group vibration of organic compounds on the OZONp surface through FTIR analysis (subsection 3.3). Those surface-bound phytochemicals can alter the electronic band structure of ZnO by forming surface states, which affects charge carrier dynamics to act as photosensitizers, which may extend light absorption to the visible range, by ligand-to-metal charge transfer. It can also influence the morphology and surface area of nanoparticles (as in SEM analysis), which in turn affects the availability of active sites. It can also act as electron shuttles or reactive oxygen species (ROS) stabilizers in photocatalysis The computational analysis was thus done to determine the phytochemicals that have the electronic properties that are conducive to these surface modification effects. Knowledge of the frontier molecular orbitals, electron-donating/-accepting properties, and reactive sites of compounds, such as ferulic acid, hesperidin, and narirutin, explains: (a) why some morphologies (nanoflowers vs. nanorods) develop at a certain concentration of the precursor, (b) how the blue-shifted UV absorption and other 400 nm band may be formed, and (c) how synergies could be observed between ZnO and surface-bound organics under photocatalysis. The association of computational descriptors (especially electrophilicity index and chemical softness) and the experimental photocatalytic activity is a separate indicator that phytochemical electronic characteristics have a role in the functionality of the resulting OZONp composite material, which is the essence of the hypothesis. The extract of orange peel, consisting of

heaps of bioactive compounds, acts as a reducing as well as stabilizing agent during the green synthesis of OZONp. Out of numerous phytochemicals, four major constituents, namely, limonene, ferulic acid, hesperidin, and narirutin (Figure 7), were considered in detail to examine electronic structure properties that may contribute to the nanoparticle formation and the catalytic performance.

In order to understand their potential, we have conducted the frontier molecular orbital (FMO) analysis, where we have considered the HOMO, and LUMO energy levels and their calculated differences (energy gap, 18Eg). Such parameters provide details involved in the chemical reactivity of each compound, as well as its electron transportation abilities that are essential in mediating the formation of nanoparticles and catalyzing the photodegradation of pollutants. Compared to others, limonene had the highest HOMOLUMO gap (9.44 eV) and HOMO (or LUMO) energy of -8.07 (or 1.38) eV (Figure 10, Table 3) that limited chemicals that are chemically stable and low in reactivity. Although this indicates that limonene can offer mechanical strength when making nanoparticles, it is unlikely to play an active role in the electron transfer or redox processes essential to boosting photocatalysis. Ferulic acid, hesperidin and narirutin on the other hand had smaller energy gaps of 6.52 eV, 6.56 eV and 6.91 eV respectively meaning that they will be more reactive. Both flavonoid glycosides, a Hesperidin and Narirutin have many hydroxyl groups and π - elongated conjugation, allowing more effective electron delocalization. Their HOMO and LUMO orbitals are dispersed on aromatic rings which can facilitate effective interaction with Zn^{2+} ions when binding nanoparticles of ZnO forming, thus providing smaller and more active catalytic nanoparticles of ZnO. Quantum chemical descriptors are also calculated in order to investigate further their redox behavior. Ferulic acid was the only compound with the electron affinity (1.02 eV) that was the highest and a very high ionization potential (7.54 eV), which implied that the compound possessed great ability to both donate and accept electrons, an important property demonstrated by redox-active agents. Limonene, however, had low favorable EA (1.38 eV), indicating its higher tendency to give electrons instead, but its disinclination to accept electrons, according to its limited usefulness in redox chemistry reactions. Table 3 showed that the above findings were consistent with the trend of chemical hardness (η) and softness (σ), supported by the fact limonene was the hardest (η = 4.72 eV) and ferulic acid the softest molecule (η = 3.26 eV), favoring the exchange of electrons. Correspondingly, the values of electronegativity (χ) were also higher in ferulic acid (4.28 eV) and narirutin (4.08 eV) thus these compounds proved to have higher tendencies to attract electron and moderate metal ions in the synthesis process. Compared in the electrophilicity index (o), a listing of the propensity of a molecule capturing electrons, ferulic acid (2.81 eV) recorded the highest followed by narirutin (2.42 eV), hesperidin (2.30 eV) and limonene (1.18 eV). These values indicate that ferulic acid specifically, could serve well as nucleating and stabilizing agents of ZnO. All in all, the electronic characteristics of ferulic acid, hesperidin, and narirutin make them the most restful candidates in orange peel extract to allow the formation of the ZnO nanoparticles. Their desirable redox properties and molecular softness are most probable to be a factor in increasing the decomposition of methylene blue dye via photocatalysis, especially in the light-aided case.

3.7.2. Molecular electrostatic potential (ESP)

To better understand how the main phytochemicals in orange peel contribute to the green synthesis of zinc oxide nanoparticles (ZnO-NPs), we analyzed the molecular electrostatic potential (ESP) maps of limonene, ferulic acid, hesperidin, and narirutin (Figure 11). The distributions of electrons in each molecule are visually presented in these maps, allowing possible reactive sites to be identified especially on the most probable interactions of the compounds with zinc ions (Zn^{2+}). The ESP maps refer to the electron-rich (in red) regions that can be nucleophilic centres or be electron-poor (in blue) which are electrophilic centres. These differences aid in locating where electrostatic attractions, hydrogen bonding or coordination to metal ions such as Zn^{2+} are most apt to occur. Limonene has a fairly smooth ESP surface, and mostly green to blue zones and almost no red zones are present. This indicates that it is weak in imparting that electron-donating effect, probably because it does not contain any oxygen-containing functional groups. This fact is agreed on by its large HOMO-LUMO energy gap (9.44 eV) and low electronegativity (e = 3.34 eV) which imply that limonene is not likely to have a powerful chelating action. It is probably more useful as a stabilizer or support matrix when constructing ZnO nanoparticles. Ferulic acid, however, indicates strong red areas at its carboxylic acid and hydroxyl math groups, which have been found to coordinate well with a metal ion. Ferulic acid has a smaller HOMO-LUMO gap (6.52 eV) and lesser electronegativity (x = 4.28 eV), which means that this compound is more reactive and therefore in a better situation to produce electrons which can assist nucleation and growth of ZnO particles. Both of these flavonoid glycosides, hesperidin and narirutin, have huge electron-enriched areas, especially those related to several hydroxyl and ether oxygen atoms. Such a large area of red and orange spots in their ESP surfaces indicates great potential in their ability to bind and reduce metal ions. They have the properties of agreement between electron delivery and acceptance, including moderate chemical hardness and electrophilicity (2.30 eV hesperidin and 2.42 eV narirutin). This coupling is paramount both to the reduction of the Zn^{2+} to nanoparticles and also the stabilization of the resulting nanoparticles. Besides, their conjugated aromatic systems can upraise photocatalytic degradation of MB dye by transferring electrons in light exposure. In summary, the ESP profiles and quantum descriptors serve together to demonstrate different contributions these phytochemicals make in the synthesis of the nanoparticle and its photocatalytic properties, such as structural support (limonene) to active reduction and stabilization (ferulic acid, hesperidin, narirutin).

4. Conclusion

This experiment was able to exhibit the sustainable preparation of zinc oxide nanoparticles (OZONp) under a

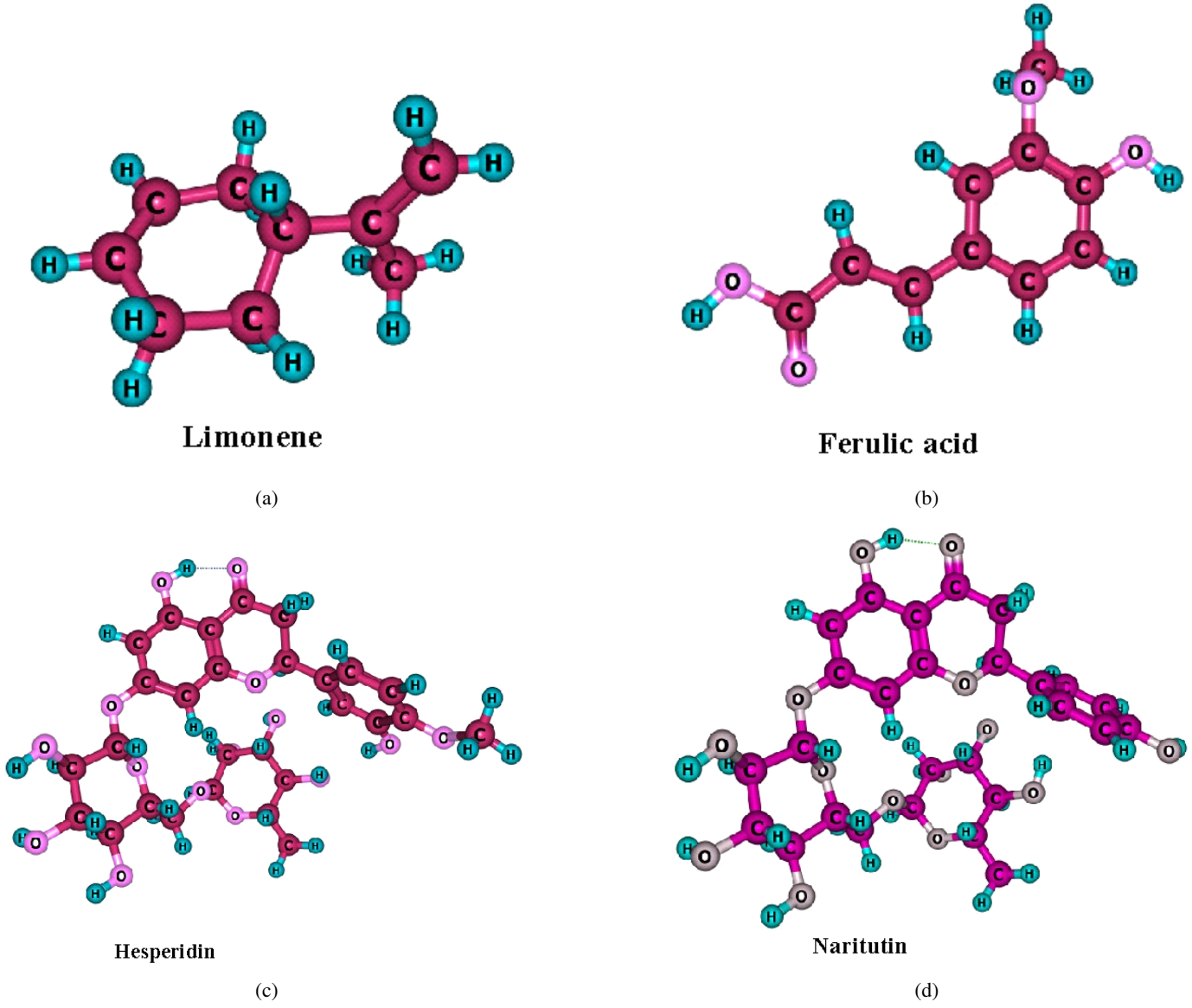

Figure 9: (a-d) 3D structures of the major phytochemicals in orange peel at m06-2x/def2TZVP level of theory.

green route using the Citrus sinensis (orange) peel extract and assess their photocatalytic activity in the degradation of methylene blue dye. The study offers useful information on green nanotechnology in mitigating environmental pollution as well as adding value to the concepts of the circular economy by providing agricultural waste with a second life.

OZONp were efficiently prepared under different concentrations of zinc salt (0.01-0.1 M) with the help of orange peel extract as a precipitating and stabilizing factor. The presence of nanoparticle formation as established by UV-Vis spectroscopy with typical absorption bands of 250-280 nm, which follows a blue-shift effect of bulk ZnO (350-380 nm), is a pointer of nanoscale dimensions and effective capping effect by the phytochemicals. The FTIR results confirmed the occurrence of bioactive functional groups (O-H, C=O, C-N, C=C, Zn-O) in the surfaces of the nanoparticles, which confirmed the role played by orange peel phytochemicals in the synthesis and the surface modification.

SEM analysis showed that the morphological evolution was obvious, concentration-dependent with irregular aggregates at 0.01 M, nanorods at 0.03 M, hierarchical nanoflowers at 0.05-0.1 M. The morphological shift of this type indicates a dynamic intertextuality in the interaction of nucleation kinetics, ionic availability, as well as interaction of bio-organic capping agents in the green synthesis process. These nanoflower shapes at larger concentrations of the precursors displayed substructures of petals, indicating that hierarchical self-assembly took place via phytochemical effects of templating.

Photocatalytic degradation experiments indicated the

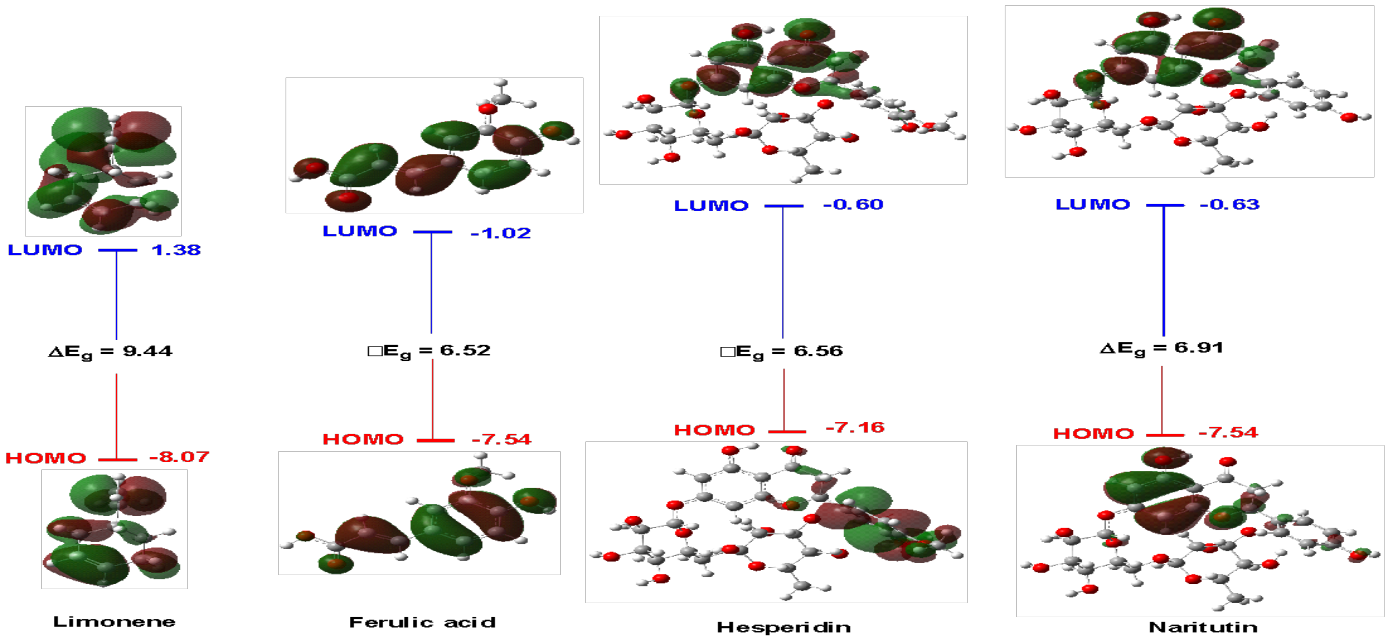

Figure 10: The LUMO, HOMO and HOMO–LUMO energy gap of some key phytochemicals in orange peel.

Table 3: Quantum chemical descriptors of some selected orange peel phytochemicals.

Compound	Limonene	Ferulic acid	Hesperidin	Narirutin
ELUMO (eV)	1.38	-1.02	-0.6	-0.63
EHOMO (eV)	-8.07	-7.54	-7.16	-7.54
ΔEg (eV)	9.44	6.52	6.56	6.91
EA (eV)	-1.38	1.02	0.6	0.63
IP (eV)	8.07	7.54	7.16	7.54
η (eV)	4.72	3.26	3.28	3.45
σ (eV^{-1})	0.21	0.31	0.3	0.29
μ (eV)	-3.34	-4.28	-3.88	-4.08
χ (eV)	3.34	4.28	3.88	4.08
ω (eV)	1.18	2.81	2.3	2.42

presence of concentration-dependent patterns of performance. Currently, efficiencies were found to be 40.0-44.0 % at 60 minutes of natural sunlight exposure, with the highest efficiencies of 0.1 M OZONp being 44 %. Kinetic studies revealed an appearance of pseudo-first-order behavior at low concentrations of dyes (5 mgL^{-1} $R^2 \geq 0.99$) and a maximum rate constant of 0.0384 min^{-1} using 0.1M OZONp to degrade 10 mgL^{-1} MB. These findings are comparable and even better than other biogenically produced ZnO photocatalysts found in the recent literature, especially in light of using natural sunlight instead of controlled UV irradiation.

The rate constant against the concentration of zinc salts, graphical analysis showed that there were specific trends in all MB loadings. The MB series of 10 mgL^{-1} showed the most significant response (5-fold increase), and this suggests there are optimal conditions of dye to catalyst ratios where the morphological improvement directly correlates with the photocatalytic performance. Conversely, the performance at 5 mgL^{-1} did not change much (catalyst excess), whereas performance at 50 mgL^{-1} exhibited subdued changes (mass transfer and light screening constraints). The unusual activity at 20 mgL^{-1} MB when 0.03 M OZONp (rod morphology) represents the paramount significance of aligning the catalyst morphology with the specific application needs.

Calculations with density functional theory have given the identification of ferulic acid, hesperidin, and narirutin as the main phytochemicals in orange peel extract with good electronic properties to be used in synthesizing nanoparticles and probably improving photocatalysis. These compounds were characterized by medium HOMO-LUMO energy gaps (6.52-6.91 eV), chemical softness (s = 0.29-0.31 eV^{-1}) and a high level of electrophilicity (o = 2.30-2.81 eV), indicating that they can coordinate with metal ions, stabilize nanoparticle surfaces, and could affect the electron transfer mechanisms in the process of photocatalysis The molecular electrostatic potential maps indicated the presence of electron rich areas

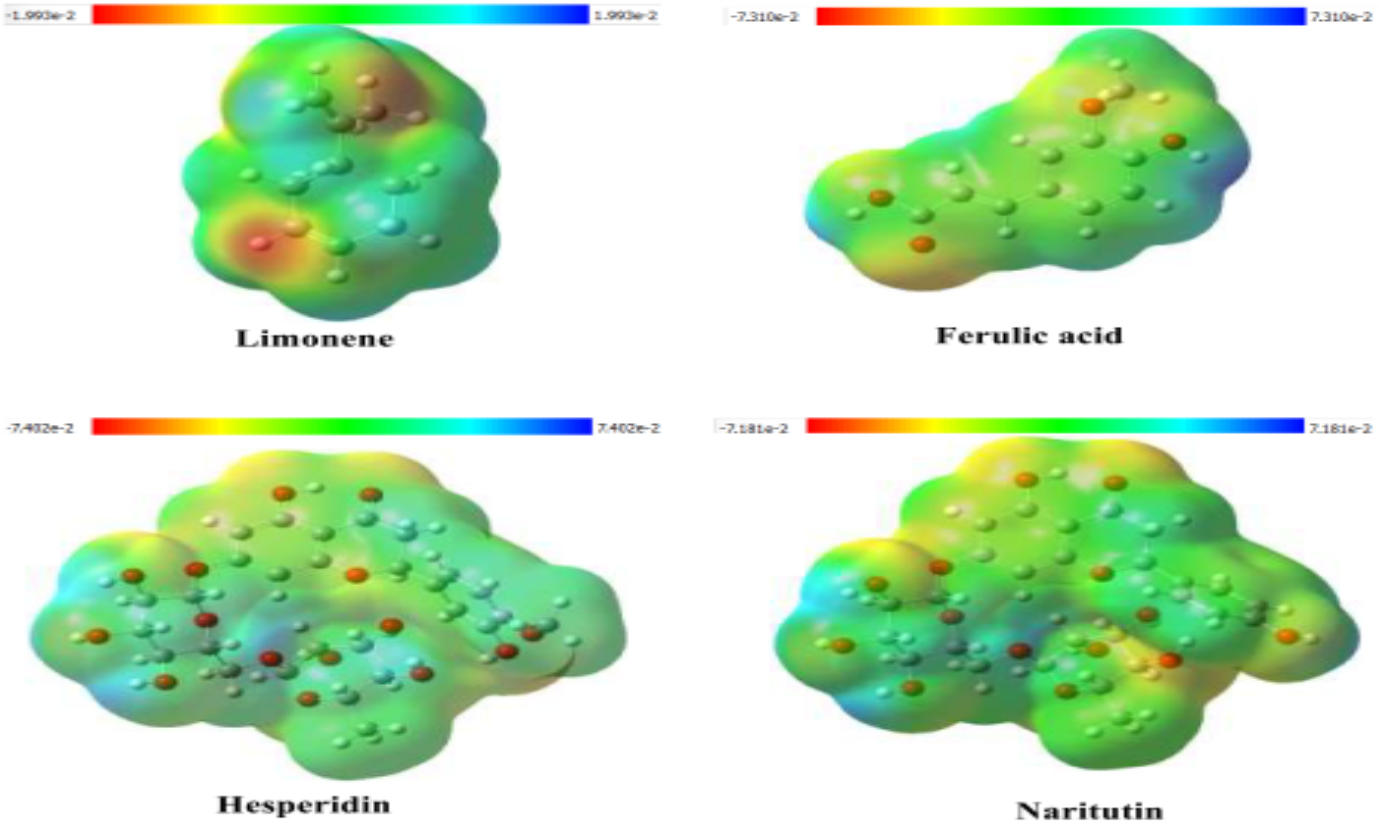

Figure 11: : Electrostatic potential surface maps of limonene, ferulic acid, hesperidin, and narirutin showing electron-rich (red) and electron-poor (blue) regions. The maps were generated using an isovalue of 0.02 a.u.

on hydroxyl and carboxyl groups and this explains the reason they have a high binding affinity to Zn^{2+} ions and capped the surface of OZONp, subsequently.

The proposed study seeks to address two key issues of environmental concern at the same time, namely (i) the remediation of toxic synthetic dye contaminants in aquatic environments, and (ii) the utilization of agricultural waste (orange peels) that would otherwise add to the landfill load. The fact that natural sunlight is used as the source of photons also improves the sustainability profile, as it does not need energy expenditures, which are required to power the artificial UV lamps, and the method is specifically appealing to the developing regions where the solar resources are abundant.

The research confirms the use of orange peel extract as a bio-reagent in the synthesis of ZnO nanoparticles and proves that phytochemicals of plant origin could be used instead of dangerous chemical reducing agents and synthetic stabilizers. The technology removes the generation of toxic byproducts, lowers synthesis expenses, lowers the temperature of the reaction (60 °C compared to > 500 °C in physical procedures), and may not necessitate any specific equipment, enabling the transfer of the technology to settings with resource limitations.

This study uses a combination of experimental characterization and computational quantum chemistry to offer insights into the molecular mechanics governing particular phytochemicals and their effects on the formation and properties of nanoparticles. The relationship between phytochemical electronic descriptors and experimentally measured photocatalytic performance bridges the gap between green synthesis and functional material design and provides a guide in the future of nanoparticle synthesis with bio-reagents to rational selection of the bio-reagent to be used.

The presented photocatalytic activity (40-44% degradation in 60 minutes) under natural sunlight provides the possibility of practical implementation of the technology in wastewater treatment. The strength of the synthesis technique with varying concentrations of precursors (all yielding functional photocatalysts) reflects the flexibility of the process that can be scaled to a larger size and put into industrial use. The determination of the optimum conditions (0.1 M precursor, 10 mgL^{-1} dye) gives actionable parameters on how the process is designed.

Data availability

The dataset used in this study is available upon request to the corresponding author.

References

[1] D. Bhatia, N. R. Sharma, J. Singh & R. S. Kanwar, "Biological methods for textile dye removal from wastewater: a review", Critical Reviews in Environmental Science and Technology **47** (2017) 183. https://doi.org/10.1080/10643389.2017.1393263.

[2] P. Dutta, M. R. Rabbi, M. A. Sufian & S. Mahjebin, "Effects of textile dyeing effluent on the environment and its treatment: a review", Engineering and Applied Science Letters **5** (2022) 1. https://doi.org/10.30538/psrp-easl2022.0080.

[3] O. Akinsipo, A. Osinubi & B. Adebayo,"Green synthesis and characterization of zinc oxide nanoparticles using euphorbia lateriflora leaf extract: evaluation of antimicrobial and antioxidant activities", FUDMA Journal of Sciences **10** (2026) 45. https://doi.org/10.33003/fjs-2026-1002-4456.

[4] R. Sangamnere, T. Misra, H. Bherwani, A. Kapley & R. Kumar, "A critical review of conventional and emerging wastewater treatment technologies", Sustainable Water Resources Management **9** (2023) 58. https://doi.org/10.1007/s40899-023-00829-y.

[5] A. Mojiri, "Treatment of water and wastewater: challenges and solutions", Separations **10** (2023) 385. https://doi.org/10.3390/separations10070385.

[6] A. Ayub, A. K. Wani, C. Chopra, D. K. Sharma, O. Amin, A. W. Wani, A. Singh, S. Manzoor & R. Singh, "Advancing dye degradation: integrating microbial metabolism, photocatalysis, and nanotechnology for eco-friendly solutions", Bacteria **4** (2025) 15. https://doi.org/10.3390/bacteria4010015.

[7] D. Kirubakaran, J. B. Abdul Wahid, N. Karmegam, R. Jeevika, L. Sellapillai, M. Rajkumar & K. J. SenthilKumar, "A comprehensive review on the green synthesis of nanoparticles: advancements in biomedical and environmental applications", Biomedical Materials & Devices **4** (2025) 388. https://doi.org/10.1007/s44174-025-00295-4.

[8] S. O. Alayande, A. A. Akinsiku, O. B. Akinsipo (Oyelaja), E. O. Ogunjinmi & E. O. Dare, Green synthesized silver nanoparticles and their therapeutic applications. In S. K. Verma & A. K. Das (Eds.), *Comprehensive analytical chemistry*, Elsevier **94** 2021 585. https://doi.org/10.5772/intechopen.1002203.

[9] M. M. Abomughaid, "Bio-fabrication of bio-inspired silica nanomaterials from orange peels in combating oxidative stress", Nanomaterials **12** (2022) 3236. https://doi.org/10.3390/nano12183236.

[10] Y. Zhao & D. G. Truhlar, "The M06 suite of density functionals for main group thermochemistry, thermochemical kinetics, noncovalent interactions, excited states, and transition elements", Theoretical Chemistry Accounts **120** (2008) 215. https://doi.org/10.1007/s00214-007-0310-x.

[11] F. Weigend,"Accurate Coulomb-fitting basis sets for H to Rn", Physical Chemistry Chemical Physics **8** (2006) 1057. https://doi.org/10.1039/b515623h.

[12] R. Dennington, T. Keith, J. Millam, K. Eppinnett, W. Hovell & R. Gilliland, GaussView, version 6, Semichem Inc., Shawnee Mission, KS, USA, 2016.

[13] Chemcraft - graphical software for visualization of quantum chemistry computations, Version 1.8, build 682. https://www.chemcraftprog.com.

[14] M. Miar, A. Shiroudi, K. Pourshamsian, A. R. Oliaey & F. Hatamjafari, "Theoretical investigations on the HOMO–LUMO gap and global reactivity descriptor studies, natural bond orbital, and nucleus-independent chemical shifts analyses of 3-phenylbenzo[d]thiazole-2(3H)-imine and its para-substituted derivatives: Solvent and substituent effects", Journal of Chemical Research **45** (2021) 147. https://doi.org/10.1177/1747519820932091.

[15] K. Fukui, T. Yonezawa & H. Shingu, "A molecular orbital theory of reactivity in aromatic hydrocarbons", Journal of Chemical Physics **20** (1952) 722. https://doi.org/10.1063/1.1700523.

[16] A. A. Ogunlana, J. Zou & X. Bao, "insights into the mechanisms and chemoselectivities of carbamates and amides in reactions involving rh(ii)-azavinylcarbene: a computational study", The Journal of Organic Chemistry **84** (2019) 8151. https://doi.org/10.1021/acs.joc.9b01070.

[17] A. A. Badeji, M. T. Omoniyi, T. B. Ogunbayo, S. D. Oladipo & I. A. Akinbulu, "quantum chemical investigation of the degradation of acid orange 7 by different oxidants", Discover Chemistry **1** (2024) 55. https://doi.org/10.1007/s44371-024-00059-x.

[18] A. Asghar, M. M. Bello, A. A. A. Raman, W. M. A. W. Daud, A. Ramalingam & S. B. M. Zain, "predicting the degradation potential of acid blue 113 by different oxidants using quantum chemical analysis", Heliyon **5** (2019) e02396. https://doi.org/10.1016/j.heliyon.2019.e02396.

[19] M. Karelson, V. S. Lobanov & A. R. Katritzky, "quantum-chemical descriptors in qsar/qspr studies", Chemical Reviews **96** (1996) 1027. https://doi.org/10.1021/cr950202r.

[20] C. G. Zhan, J. A. Nichols & D. A. Dixon, "ionization potential, electron affinity, electronegativity, hardness, and electron excitation energy: molecular properties from density functional theory orbital energies", The Journal of Physical Chemistry A **107** (2003) 4184. https://doi.org/10.1021/jp0225774.

[21] R. G. Parr, L. v. Szentpály & S. Liu, "electrophilicity index", Journal of the American Chemical Society **121** (1999) 1922. https://doi.org/10.1021/ja983494x.

[22] S. D. Oladipo, S. J. Zamisa, A. A. Badeji, M. A. Ejalonibu, A. A. Adeleke, I. A. Lawal, A. Henni & M. M. Lawal, "Ni^{2+} and Cu^{2+} complexes of N-(2,6-dichlorophenyl)-N-mesityl formamidine dithiocarbamate structural and functional properties as CYP3A4 potential substrate", Scientific Reports **13** (2023) 13414. https://doi.org/10.1038/s41598-023-39502-x.

[23] L. Liu, J. Feng, Y. Liu, Y. Wu & S. Liu, "Molecular electrostatic potential: A new tool to predict the lithiation process of organic battery materials", The Journal of Physical Chemistry Letters **9** (2018) 3573. https://doi.org/10.1021/acs.jpclett.8b01123.

[24] G. Náray-Szabó, "Preferred channels for nucleophilic and electrophilic attack from simple molecular potential maps", Acta Physica Academiae Scientiarum Hungaricae **51** (1981) 65. https://doi.org/10.1007/BF03155565.

[25] C. H. Suresh, G. S. Remya & P. K. Anjalikrishna, "Molecular electrostatic potential analysis: A powerful tool to interpret and predict chemical reactivity", Wiley Interdisciplinary Reviews: Computational Molecular Science **12** (2022) e1601. https://doi.org/10.1002/wcms.1601.

[26] V. B. Sumithranand, M. S. Roxy & G. Vaishnavi, "Green synthesis of ZnO nanoparticles using sweet orange peels as a mediating agent and their antibacterial properties", Oriental Journal of Chemistry **40** (2024) 221. https://doi.org/10.13005/ojc/400221.

[27] A. Anik, M. A. Alam, M. Alam, D. Sarker & N. Sultana, "Photocatalytic degradation of methylene blue dye using bio-green synthesis of ZnO nanoparticles from Justicia adhatoda leaves extract", SSRN (2024). https://doi.org/10.2139/ssrn.5260651.

[28] I. Khan, K. Saeed & I. Khan, "Nanoparticles: Properties, applications and toxicities", Arabian Journal of Chemistry **12** (2019) 908. https://doi.org/10.1016/j.arabjc.2017.05.011.

[29] E. I. Oikeh, F. E. Oviasogie & E. S. Omoregie, "Quantitative phytochemical analysis and antimicrobial activities of fresh and dry ethanol extracts of Citrus sinensis (L.) Osbeck (sweet Orange) peels", Clinical Phytoscience **6** (2020) 46. https://doi.org/10.1186/s40816-020-00193-w.

[30] M. Bayat, M. Zargar, T. Astarkhanova, E. Pakina, S. Ladan, M. Lyashko & S. I. Shkurkin, "Facile biogenic synthesis and characterization of seven metal-based nanoparticles conjugated with phytochemical bioactives using fragaria ananassa leaf extract", Molecules **26** (2021) 3025. https://doi.org/10.3390/molecules26103025.

[31] K. R. S. Murthy, G. K. Raghu & P. Binnal, "Zinc oxide nanostructured material for sensor application", Journal of Biotechnology and Bioengineering **5** (2021) 25. https://doi.org/10.22259/2637-5362.0501004.

[32] A. Rashid Salah, I. Ibraheem, J. Khalil, A. Naser & S. Mohammad Salim, "Sustainable-green synthesis and characterization of zno nanoparticles and evaluation of their antibacterial and antioxidant activities", Journal of Nanostructures **15** (2025) 180. https://doi.org/10.22052/JNS.2025.01.017.

[33] H. Xu, H. Wang, Y. Zhang, W. He, M. Zhu, B. Wang & H. Yan, "Hydrothermal synthesis of zinc oxide powders with controllable morphology", Ceramics International **30** (2004) 93. https://doi.org/10.1016/S0272-8842(03)00069-5.

[34] S. Jayswal & R. S. Moirangthem, "Fabrication of hierarchical hybrid zno/au micro-/nanostructures for efficient dye degradation: role of gold nanostructures in photophysical process", Colloids and Surfaces A: Physicochemical and Engineering Aspects **630** (2021) 127555. https://doi.org/10.1016/j.colsurfa.2021.127555.

[35] N. Talebian, S. M. Amininezhad & M. Doudi, "Controllable synthesis of ZnO nanoparticles and their morphology-dependent antibacterial and optical properties", Journal of Photochemistry and Photobiology B: Biology **120** (2013) 66. https://doi.org/10.1016/j.jphotobiol.2013.01.004.

[36] E. S. Hadi & K. K. Jasim, "Responsive uv-light photocatalytic of Ag/ZnO nanocomposites for removal of brilliant blue dye: as a model for advanced chemical studies", Advanced Journal of Chemistry—Section A **8** (2025) 604. https://doi.org/10.48309/ajca.2025.474706.1654.

[37] L. N.S. J. Lee, H. J. Jung, R. Koutavarapu, S. H. Lee, M. Arumugam, J. H. Kim & M. Y. Choi, "ZnO supported Au/Pd bimetallic nanocomposites for plasmon improved photocatalytic activity for methylene blue degradation under visible light irradiation", Applied Surface Science **496** (2019) 143665. https://doi.org/10.1016/j.apsusc.2019.143665.

[38] N. J. I. Groeneveld, M. Kanelli, F. Ariese & M. R. van Bommel, "Parameters that affect the photodegradation of dyes and pigments in solution and on substrate—an overview", Dyes and Pigments **210** (2023) 110999. https://doi.org/10.1016/j.dyepig.2022.110999.

[39] S. Jayswal & R. S. Moirangthem, "Fabrication of hierarchical hybrid zno/au micro-/nanostructures for efficient dye degradation: role of gold nanostructures in photophysical process", Colloids and Surfaces A: Physicochemical and Engineering Aspects **630** (2021) 127555. https://doi.org/10.1016/j.colsurfa.2021.127555.

[40] E. S. Hadi & K. K. Jasim, "Responsive UV-light photocatalytic of Ag/ZnO nanocomposites for removal of brilliant blue dye: as a model for advanced chemical studies", Advanced Journal of Chemistry, Section A **8** (2025) 604. https://doi.org/10.48309/AJCA.2025.474706.1654.

[41] P. Singla, O. P. Pandey & K. Singh, "Study of photocatalytic degradation of environmentally harmful phthalate esters using Ni-doped TiO2 nanoparticles", International Journal of Environmental Science and Technology **13** (2016) 849. https://doi.org/10.1007/s13762-015-0909-8.

[42] A. Anik, M. A. Alam, M. Alam, D. Sarker & N. Sultana, "Photocatalytic degradation of methylene blue dye using bio-green synthesis of ZnO nanoparticles from justicia adhatoda leaves extract", SSRN (2024). https://doi.org/10.2139/ssrn.5262386.

[43] A. S. Rashid, I. K. Ibraheem, J. A. Naser & S. S. Mohammad, "Sustainable-green synthesis and characterization of zno nanoparticles and evaluation of their antibacterial and antioxidant activities", Journal of Nanostructures **15** (2025) 180. https://doi.org/10.22052/JNS.2025.01.017.

[44] S. J. Lee, H. J. Jung, R. Koutavarapu, S. H. Lee, M. Arumugam, J. H. Kim & M. Y. Choi, "ZnO supported Au/Pd bimetallic nanocomposites for plasmon improved photocatalytic activity for methylene blue degradation under visible light irradiation", Applied Surface Science **496** (2019) 143665. https://doi.org/10.1016/j.apsusc.2019.143665.

[45] I. Groeneveld, M. Kanelli, F. Ariese & M. R. van Bommel, "Parameters that affect the photodegradation of dyes and pigments in solution and on substrate – an overview", Dyes and Pigments **210** (2023) 110999. https://doi.org/10.1016/j.dyepig.2022.110999.

[46] K. M. Lee, C. W. Lai, K. S. Ngai & J. C. Juan, "Recent developments of zinc oxide based photocatalyst in water treatment technology: A review", Water Research **88** (2016) 428. https://doi.org/10.1016/j.watres.2015.09.045.